

Emission-Line Fluxes of Northern Planetary Nebulae

N. Aksaker^{1*}, S. K. Yerli², Ü Kızıloğlu², and B. Atalay³

¹ Vocational School of Technical Sciences, University of Çukurova, Adana, Turkey

² Orta Doğu Teknik Üniversitesi, Department of Physics, Ankara, Turkey

³ Atatürk University, Faculty of Science, Department of Physics, Erzurum, Turkey

Abstract

We present long slit spectrophotometric emission line fluxes of bright and extended (<5 arcsec in diameter) Planetary Nebulae (PNe) selected from [Acker et al. 1992](#) catalog with suitable equatorial coordinates for Northern hemisphere. In total, 17 PNe have been chosen and observed in 2008–2010. To measure absolute fluxes, broad slit sizes, ranging from $3.5''$ to $7.5''$ were used and thus equivalent widths of all observable emission line fluxes were also calculated. Among 17 PNe's observed, line flux measurements of 12 of them were made for the first time. This work also aims to extend the sky coverage of emission line flux standards in Northern hemisphere ([Dopita & Hua 1997](#) - 52 PNe in Southern hemisphere; [Wright et al. 2005](#) - 6 PNe in Northern hemisphere). Electron temperatures and densities, and chemical abundances of these PNe were also calculated in this work. These data is expected to lead the photometric or spectrometric further work for absolute emission line flux measurements needed for H II regions, supernova remnants etc.

Keywords: planetary nebulae: general; techniques: spectroscopic

1 Introduction

Studying the stellar evolution in terms of chromospheric activities and kinematics of stars themselves within the Galaxy could also impact on what we know about planetary nebulae (PNe) i.e. when the star's interiors are completely revealed with enriched matter content which will be fed to interstellar medium (ISM) with stellar wind, and therefore enriching the ISM. The key point in these studies lie in the spectroscopic observations of PNe when accurate emission line fluxes are measured ([Madsen et al. 2006](#)). Moreover, with the help of this knowledge we can understand how these regions are related to the general structure of the ISM.

In the past there were several works that they have relied on standard star observations using broad band photometry or spectrophotometry, or even using photon counting detectors. However, these observations help little in improving the emission line flux standards of PNe, HII regions, cataclysmic variables, supernova remnants, etc. ([Wright et al. 2005](#)). For photon counting coupled with interference filters: [Liller 1955](#); [O'Dell 1963](#); they had several large error sources such as unknown central wavelength of transmission curves, temperature variations, filter age and misalignment of various optical components. For broad band photometry ([Johnson & Harris 1954](#); [Landolt 1992](#)) and spectrophotometry: ([Stone & Baldwin 1983](#); [Massey et al. 1988](#);

*Correspondence address: naksaker@cu.edu.tr

Oke 1990); even though there are many type of standard stars available, the flux standards of emission lines are still not adequate in number. In addition to this, several emission and absorption lines coincide in continuum standards (e.g. Balmer series) and when narrow band filters are used, exact contribution of the line fluxes would be difficult. Contrary to abovementioned observation methods, using low read-out noise and high quantum efficiency CCDs, spectrophotometry of emission lines of PNe's could very accurately be measured even for faint sources.

Therefore, high precision photometric studies of the emission line fluxes of ionized nebulae are needed.

Lately, Dopita & Hua 1997 (hereafter D97) made slitless spectrophotometric observation of southern compact PNe chosen from the catalog of Acker et al. 1992 (hereafter A92). They gave $H\alpha$, $H\beta$, O III and laboratory wavelengths of N II and S II emission lines for 39 PNe. For northern hemisphere sources Wright et al. 2005 (hereafter W05) presented all emission lines of only 6 PNe using similar techniques. Although this was off to a good start, it is not sufficient for northern hemisphere.

By increasing the northern hemisphere sources to 17 with this work, a complete set of emission line standards will be builded up for both hemisphere.

2 Observations

The catalog of A92 includes 1142 PNe. Therefore, it is used as the main source of our work. The PNe to be observed were selected according to the following criteria:

- To select only northern hemisphere PNe, first declination is limited to $\delta > -35^\circ$ which reduces the total number to 838.

- Then, RA in between 7^h and 12^h are excluded from the selection which reduces the total number to 805 PNe.
- From this subset, angular size of PNe smaller than 5 arcsecond are selected (i.e. PNe fits to the available slit size). This reduced the total number to 276 PNe.
- Then, less studied 12 PNe were selected.
- 5 PNe which were studied by W05 were added to this subset increasing the total number to 17.

Journal of observations for the selected PNe are given in Table 1.

Sky distribution of target list given in Table 1 is shown in Figure 1. It contains sources of both D97 and W05. It can easily be seen from the figure that our aim of filling sky coverage gaps in northern hemisphere is achieved.

The observations were performed with the TFOSC¹ (TÜBİTAK Faint Object Spectrometer and Camera) coupled with the 150 cm Russian-Turkish Telescope (RTT150). The camera is equipped with a 2048x2048 (15 μm) pixel Fairchild 447BI CCD.

The mean seeing level through out the observing nights were 1.9'', ranging from 0.6'' to 2.6''. The seeing measurements were calculated from unfiltered frames by averaging over FWHM's of field stars which were taken just before the spectrum observations. The seeing characteristics of the site were well determined by Ozisik & Ak (2004).

In the spectroscopic work, mainly G7 (Grism 7: 3850-6850 Å; visible), G8 (Grism 8: 5800-8300 Å; red) and G14 (Grism 14: 3275-6100 Å; blue) were used. The average dispersions were 1.5, 1.1, and 1.4 Å/pixel for G7, G8, and G14, respectively. Considering the telescope optics and seeing conditions, an optimum Signal-to-Noise

¹<http://tug.tubitak.gov.tr/tr/teleskoplar/tfosc>

Table 1 Journal of Observations for the target list. Description of the columns are as follow. The most common object names (Column 1), Source coordinates (Column 2 and 3), R magnitude of the source given in SIMBAD (Column 4), Source diameter in arcsec (Column 5) given in A92 catalog, Total exposure for blue and red grism (Column 6) and Observation date (Column 7)

Object Name	α_{2000}	δ_{2000}	R Mag.	Diameter	Exposure	Obs. Date
	(h m s)	(d m s)		($''$)	(s)	
Hu 1-1	00 28 15.44	+55 57 54.48	-	5	3000	10 Jul. 2010
BoBn 1	00 37 16.03	-13 42 58.60	14.6	3	2400	9 Nov. 2008
M 1-4	03 41 43.37	+52 17 00.54	11.9	4	1800	11 Jul. 2010
M 1-5	05 46 50.01	+24 22 02.80	12	2	2400	9 Nov. 2008
K 3-70	05 58 45.34	+25 18 43.80	13.9	1.8	3600	9 Nov. 2008
M 1-17	07 40 22.20	-11 32 29.92	12.4	3	1200	10 Nov. 2008
SaSt 2-3	07 48 03.67	-14 07 40.40	13.1	0	1200	10 Nov. 2008
H 4-1	12 59 27.77	+27 38 10.50	14	2.7	6600	11 Jul. 2010
DdDm 1	16 40 18.15	+38 42 20.00	12.9	0.6	2400	9 Nov. 2008
Na 1	17 12 51.89	-03 15 59.69	10.9	5	4200	10 Jul. 2010
Vy 1-2	17 54 22.98	+27 59 58.10	12.4	4.6	4200	10 Jul. 2010
M 3-27	18 27 48.26	+14 29 06.10	11.9	1	2100	11 Jul. 2010
NGC 6833	19 49 46.58	+48 57 40.20	11	2	1800	10 Nov. 2008
IC 4997	20 20 08.74	+16 43 53.71	-	1.6	2100	11 Jul. 2010
IC 5117	21 32 30.97	+44 35 47.50	-	1.2	780	10 Nov. 2008
Me 2-2	22 31 43.68	+47 48 03.91	10.8	<5	180	11 Jul. 2010
Vy 2-3	23 22 57.89	+46 53 57.79	12.1	4.2	3600	10 Jul. 2010

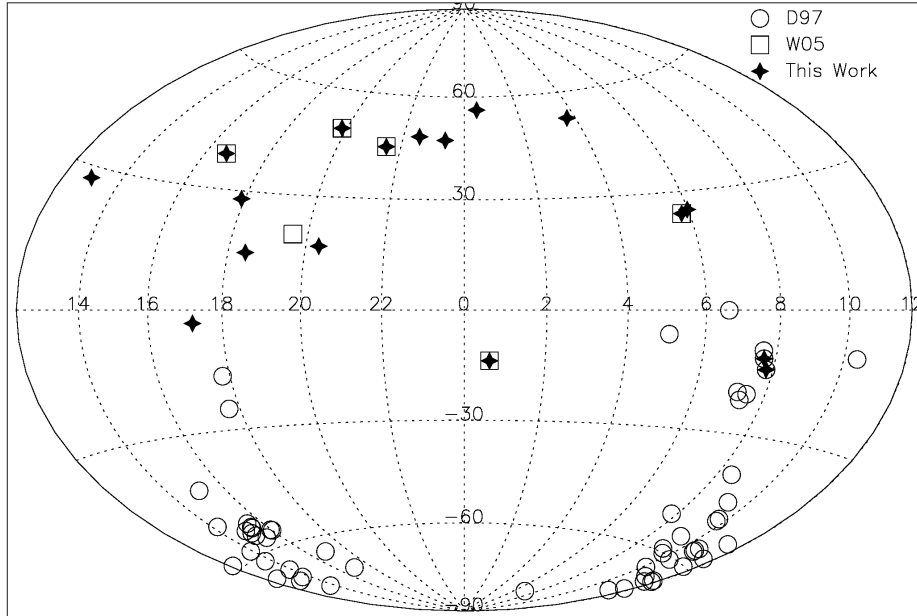


Figure 1. The sky distribution of our target list (stars) in equatorial coordinates. The source of W05 and D97 are represented by squares and circles, respectively.

Ratio (SNR) was reached with the following exposure times: 60 s for *Me 2-2* (a typical bright PNe) and 3600 s for *H 4-1* (a typical faint PNe). Note that the exposure times were determined according to source's R magnitude given in Table 1.

Each PNe was observed with a slit size which was varied according to the PNe's angular size and seeing: $3.5''$ for point-like sources and $7.3''$ for wider sources. The slit position and therefore dispersion axis is aligned to the parallactic angle to avoid loss of light due to the atmospheric refraction. Contrary to work of D97 in southern hemisphere, PNe coordinates in northern hemisphere were quite accurate: Source-to-source pointing accuracy was kept $< 5''$ and there were no loss of frames due to the autoguider failures.

3 Data Analysis

Headers of TFOSC images were processed using IDL² and then they were reduced using standard IRAF³ tasks e.g. *onedspec* and *image*. The instrumental profile of the sensor was subtracted using standard reduction packages of IRAF. The images were then converted into 1D spectra by using the *apall* task. As for the last stage wavelength and flux calibrations tasks were applied to the spectra.

To achieve a sensible accuracy in the wavelength calibration, different arc lamps were used for different grisms: He+Ne for Grism 7 (hereafter G7); Ne for Grism 8 (hereafter G8); He for Grism 14 (hereafter G14). Arc lamp atlas of ALFOSC (another spectrograph in FOSC series)⁴ were used to identify the lines in the spectra. The resultant accuracy of wavelength

calibration was around $\pm 1 \text{ \AA}$. The reference wavelength used in flux measurements are given in Tables 5-21.

Fluxes of spectrophotometric standards listed in Stone & Baldwin (1983), Baldwin & Stone (1984), Massey et al. (1988) and Oke (1990) were used in flux calibration of all PNe. The standard stars have to be identified both in one of the abovementioned catalogs and in IRAF's repository of standard stars; then the closest one to the target PNe was chosen to eliminate the effect of airmass. Finally, flux calibration tasks of IRAF (*standards*, *sensitivity*, and *calibrate*) applied to PNe images.

A typical reduced pair (red and blue) of spectra are shown in Figure 2. The bright lines in red spectrum are N II $\lambda 6548.05$, H α $\lambda 6582.85$ and N II $\lambda 6583.45$, and in blue spectrum H β $\lambda 4861.29$, O III $\lambda 5007.57$ and O III $\lambda 4959.52$.

4 Results And Discussions

The data set of each PNe is produced by measuring line flux and their equivalent widths of selected emission lines. In measuring these values background of each emission line has to be determined and then removed by a first order polynomial fit to the line extending to its wings. Background level of each emission line on the continuum was determined around the line.

The flux values and equivalent widths were then calculated by best fitting to the line. The values and their errors are given in Tables 5-21 which were computed by averaging multiple measurements of Gaussian fits of the same line. The standard deviation of the fits are then taken as the error values. All the measurements were done using standard tasks of IRAF.

Our values and values of W05 data for PNe: BoBn 1, M 1-5, NGC 6833 and IC 5117 are given in Tables 5-8, respectively. Missing values in the tables are due to the grisms having different wavelength coverages. For

²<http://www.exelisvis.com/language/en-US/ProductsServices/IDL.aspx>

³IRAF is distributed by the National Optical Astronomy Observatories, which are operated by the Association of Universities for Research in Astronomy, Inc., under cooperative agreement with the National Science Foundation.

⁴<http://www.not.iac.es/instruments/alfosc/lamps/>

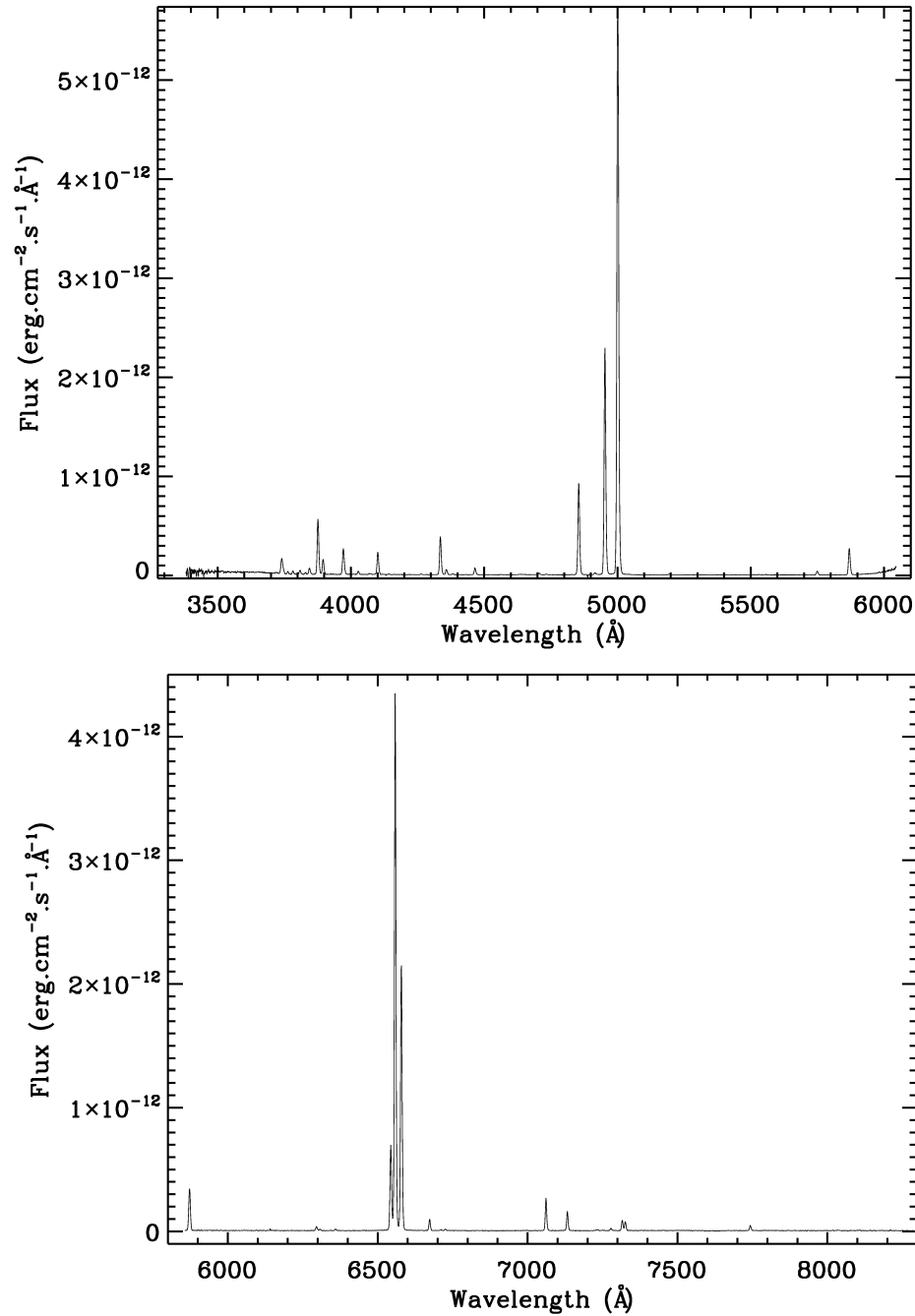


Figure 2. The blue (above panel) and red (below panel) spectra of Me 2-2.

PNe DdDm 1, however, due to having no overlapping wavelength coverage it is excluded in Table 15. Note that, He I lines are double blended in all data sets.

The corresponding error values of the data given in Tables 5-21 are around ± 0.03 dex with a standard deviation of ± 0.003 dex. To get an impression of the error

budget, percentages of flux-to-error ratios are summed over both for all the emission lines and for five bright emission lines, and they are listed in Table 2.

Number of lines detected for each object varied between 11 to 35 amounting to 375 emission lines for all objects. In addition to this in total 49 *different* emission

Table 2 The error budget of the measurements of all 17 PNe: for all emission lines (first column) and five bright lines of H α , H β , O III, N II and He I (second column).

Object Name	Total error (all lines)	Total error (bright lines)
Hu 1-1	0.2%	<0.1%
BoBn 1	0.6%	0.3%
M 1- 4	0.4%	0.3%
M 1- 5	0.5%	0.2%
K 3-70	0.2%	0.1%
M 1-17	0.1%	<0.1%
SaSt 2- 3	<0.1%	<0.1%
H 4- 1	0.2%	0.1%
DdDm 1	0.2%	<0.1%
Na 1	0.4%	0.1%
Vy 1- 2	0.2%	<0.1%
M 3-27	0.3%	0.2%
NGC 6833	0.3%	<0.1%
IC 4997	0.3%	<0.1%
IC 5117	0.2%	<0.1%
Me 2-2	0.2%	<0.1%
Vy 2- 3	0.1%	<0.1%

lines were identified where they were mostly caused by collisions (Kwok 2000, p.260) or they were the recombination lines of H I, He I and He II. However, a considerable amount of recombination lines of heavy elements were also detected such as O I, O II, O III, C IV and Ne III. In some of the sources (BoBn 1, K 3-70, DdDm 1 and M 1-4) emission lines were observed on an elevated continuum level which was due to the recombination of electrons.

Among 49 emission lines, the brightest (unsaturated) and faintest ones were the O III λ 5007.57 with -9.947 ± 0.002 from IC4997, and N II λ 6548.05 with -15.115 ± 0.080 from M 1-5, respectively. Emission line fluxes of PNe are directly proportional with optical R

magnitude of the source (see Table 1) which was also noted in this work (see Tables 5-21).

Observed H β fluxes were compared with A92 and plotted in top panel of Figure 3 (17 in total). As can be deduced from the plot, an obvious linear relation exists for both bright and faint flux arms with a R² value 0.89 on the faint arm.

A similar comparison was done for W05 including all emission lines (64 in total). However, only 4 PNe (BoBn 1, IC 5117, M 1-5, and NGC 6833) were used in the comparison (see Tables 5-8). The comparisons for flux and EW values are shown in middle and bottom panels of Figure 3, respectively. Corresponding R² values of flux and EW are 0.96 and 0.88, respectively. The deviations seen in the regression are mainly due to not resolving the faint lines.

In comparing our values with W05, there are some discrepancies which have to be mentioned in detail. The error in flux measurement of each emission line (Table 2) amounts to less than 1% of the line strength. On top this, low SNR of the spectra on relatively bad seeing conditions produced slit losses which accumulated to no more than 10% of the signal, therefore causing a relatively low flux value. However, in the absence of these negative effects a high consistency is achieved in the comparison which makes the results on the whole reliable.

Physical and chemical properties for all PNe having suitable data sets were also calculated. The analysis of the data was based on Corradi et al. 1997. Since the Balmer decrement is a sign of extinction along the observed column of ISM, extinction constant (c_{β}) were calculated using H α /H β ratio. Electron temperatures (T_e) and densities (N_e) were calculated using IRAF's nebular.temden task. Electron temperatures of T_e ([O III]) and T_e ([N II]) were calculated according to Osterbrock & Ferland (2006). Using ratio of

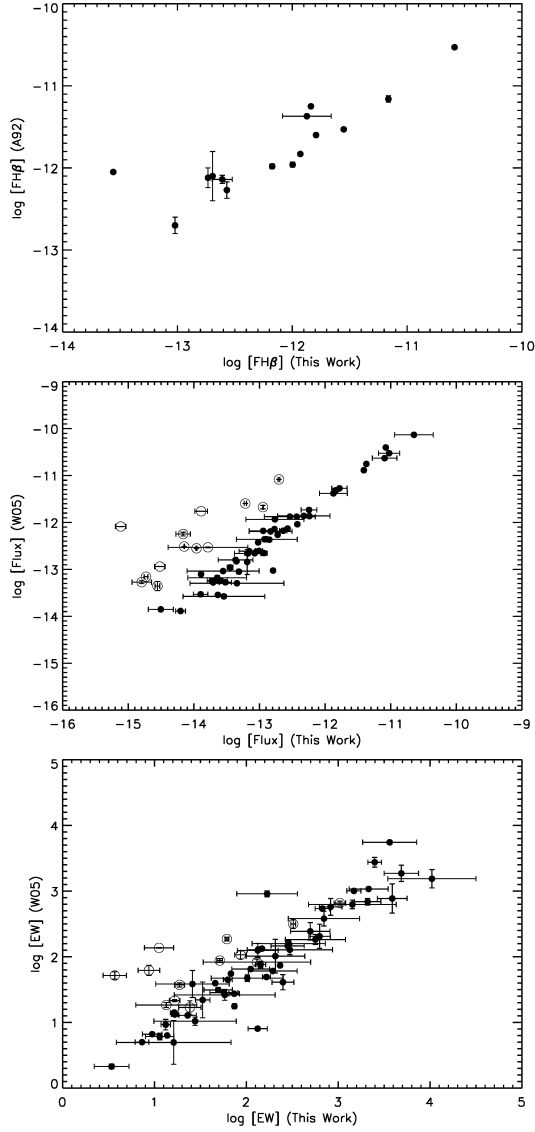


Figure 3. In the top panel a comparison of $H\beta$ fluxes of A92 (vertical) with this work (horizontal) is given. In the middle and bottom panels, a comparison of all emission line fluxes (in total 64 for 4 PNe) and EW of W05 (vertical) with this work (horizontal) are given, respectively. Open circles represent faint and blended He I lines. All axes are in log scale and fluxes are in $\text{ergs cm}^{-2} \text{s}^{-1}$.

$[\text{S II}]\lambda 6716/\lambda 6731$ and assuming an electron temperature of $T=10^4$ K, electron densities were calculated. All above calculations are given in Table 3.

For each PNe, the ionic abundances relative to Hydrogen are computed from the line fluxes relative to $H\beta$

PASA (2018)

doi:10.1017/pas.2018.xxxx

Table 3 Logarithmic extinction constant C_β , and electron temperatures and densities.

Object	C_β	$T_e([\text{O III}])$ (K)	$T_e([\text{N II}])$ (K)	$N_e([\text{S II}])$ (cm^{-3})
Hu 1-1	1.32	11 300	-	-
BoBn 1	-	12 300	-	-
M 1-4	2.20	-	-	1 100
M 1-5	1.24	-	20 300	-
K 3-70	-	-	12 200	2 100
M 1-17	1.03	-	11 900	4 000
SaSt 2-3	0.40	-	10 000	2 700
H 4-1	0.18	12 200	9 400	500
DdDm 1	-	-	-	2 100
Na 1	0.94	10 500	-	-
Vy 1-2	-	11 700	-	3 700
M 3-27	2.68	-	-	-
NGC 6833	0.04	6 000	29 600	>10 000
IC 4997	0.30	-	15 900	>10 000
IC 5117	1.22	9 900	23 700	>10 000
Me 2-2	0.37	10 500	4 500	1 700
Vy 2-3	0.34	10 400	-	-

Table 4 Ionic abundances relative to Hydrogen. All values are scaled with 10^{-6} .

Object	O I	O III	N I	N II	S II	S III	Ar IV
M 1-5	1.28	-	-	5.14	-	-	-
M 1-17	43.8	195	3.08	6.16	-	7.30	-
SaSt 2-3	18.1	1.08	-	13.5	-	-	-
H 4-1	31.7	249	2.15	18.6	6.77	-	-
NGC 6833	0.44	1770	-	16.2	0.22	0.16	-
IC 4997	-	33.7	-	2.09	-	2.05	0.06
IC 5117	3.06	29.0	-	0.69	0.33	1.21	-
Me 2-2	1.51	216	-	4550	67.6	318	4.30
Vy 1-2	-	163	-	-	-	-	-

using the temperatures and densities values given in Table 3 (see e.g. Kingsburgh & Barlow 1994; Wesson et al. 2005 for computation methods). These abundances are given in Table 4.

In calculating the values of Table 4, de-reddened fluxes have been used according to Acker (2011). In addition to this, excitation class of each PNe was also calculated according to Gurzadian & Egikian (1991) in which the nebular lines have been used as a (loosely) measure of the temperature of the central white dwarf. Note that, if the stellar nuclei of the PNe is found to be very hot then it can be taken as a *high excitation PNe*. Therefore, Hu 1-1, BoBn 1 and Vy 1-2 fall into this category. However, if some related lines are missing from the central region then a definitive calculation could not be made. Therefore the following PNe fall into this *unidentified* category: M 1-4, K3-70, M1-17 SaSt 2-3 DdDm 1 M3-27 IC 4997 and Me 2-2. Finally, the rest of the PNe can safely be classified as *medium excitation PNe*.

These studies can significantly contribute to the study of the evolution of the PNe and the Galaxy.

5 Conclusions

- A similar study of D97 (for Southern Hemisphere) and W05 (for Northern Hemisphere) have been carried out by extending the northern hemisphere coverage of PNe.
- We present new emission line fluxes to be used as a standard in both imaging in narrow band and in Fabry-Perot spectroscopy.
- Emission line flux measurements of 12 PNe were made for the first time.
- Physical and chemical properties of PNe, as well as their evolution, can be studied with continuous monitoring of these 17 PNe.
- For suitable PNe, Extinction constant, Electron Temperature, Electron Density, Chemical Abundance and Excitation Class have been calculated.

6 ACKNOWLEDGEMENTS

The authors thank to the scientific and technological research council of Turkey (TUBITAK) for a partial support in using RTT150 (Russian-Turkish 1.5-m telescope) in Antalya through with project numbers 10BRTT150-33-0 and 10ARTT150-489-0. NA also thank to TUBITAK National Observatory (TUG) staff. NA gratefully acknowledges support through a Post-Doc Fellowship from the TUBITAK-BIDEB at Physics Department of Middle East Technical University, Ankara-Turkey. The author also grateful to M. E. Ozel for reading and correcting the manuscript and for his valuable remarks.

References

- Acker, A. 2011, in EAS Publications Series, Vol. 47, EAS Publications Series, ed. J.-P. Rozelot & C. Neiner, 189–214
- Acker, A., Marcout, J., Ochsenbein, F., Stenholm, B., Tylanda, R., & Schohn, C. 1992, The Strasbourg-ESO Catalogue of Galactic Planetary Nebulae. Parts I, II.
- Baldwin, J. A. & Stone, R. P. S. 1984, MNRAS, 206, 241
- Corradi, R. L. M., Perinotto, M., Schwarz, H. E., & Claeskens, J.-F. 1997, 322, 975
- Dopita, M. A. & Hua, C. T. 1997, ApJS, 108, 515
- Gurzadian, G. A. & Egikian, A. G. 1991, Ap&SS, 181, 73
- Johnson, H. L. & Harris, D. L. 1954, ApJ, 120, 196
- Kingsburgh, R. L. & Barlow, M. J. 1994, MNRAS, 271, 257
- Kwok, S. 2000, The origin and evolution of planetary nebulae / Sun Kwok. Cambridge ; New York : Cambridge University Press, 2000. (Cambridge astrophysics series ; 33), 260
- Landolt, A. U. 1992, AJ, 104, 340
- Liller, W. 1955, ApJ, 122, 240
- Madsen, G. J., Frew, D. J., Parker, Q. A., Reynolds,

- R. J., & Haffner, L. M. 2006, in IAU Symposium, Vol. 234, Planetary Nebulae in our Galaxy and Beyond, ed. M. J. Barlow & R. H. Méndez, 455–456
- Massey, P., Strobel, K., Barnes, J. V., & Anderson, E. 1988, *ApJ*, 328, 315
- O'Dell, C. R. 1963, *ApJ*, 138, 1018
- Oke, J. B. 1990, *AJ*, 99, 1621
- Osterbrock, D. E. & Ferland, G. J. 2006, *Astrophysics of gaseous nebulae and active galactic nuclei*
- Ozisik, T. & Ak, T. 2004, 422, 1129
- Stone, R. P. S. & Baldwin, J. A. 1983, *MNRAS*, 204, 347
- Wesson, R., Liu, X.-W., & Barlow, M. J. 2005, *MNRAS*, 362, 424
- Wright, S. A., Corradi, R. L. M., & Perinotto, M. 2005, 436, 967

Table 5 BoBn 1 fluxes and equivalent widths.

Wavelength Å	Ion	This Work		W05	
		log [Flux] (ergs cm ⁻² s ⁻¹)	log [EW] (Å)	log [Flux] (ergs cm ⁻² s ⁻¹)	log [EW] (Å)
3967.41	[NeIII]	-13.680±0.008	2.719±0.240	-	-
4101.74	Hδ	-13.947±0.020	2.294±0.177	-	-
4340.47	Hγ	-13.562±0.012	2.656±0.273	-	-
4363.21	[OIII]	-14.356±0.155	1.507±0.647	-	-
4387.93	HeI	-14.368±0.014	1.830±0.216	-	-
4471.68	HeI	-14.195±0.013	2.264±0.066	-	-
4685.71	HeII	-13.891±0.019	2.124±0.222	-13.103±0.024	2.097±0.107
4861.20	Hβ	-13.021±0.007	2.917±0.124	-12.425±0.011	2.759±0.128
4958.52	[OIII]	-12.924±0.006	3.154±0.477	-12.358±0.005	2.797±0.065
5754.59	[NII]	-	-	-14.447±0.005	1.000±0.105
5007.57	[OIII]	-12.432±0.001	4.020±0.480	-11.877±0.006	3.188±0.140
5875.97	HeI	-13.706±0.023	2.316±0.320	-13.278±0.019	2.009±0.255
6300.30	[OI]	-	-	-14.503±0.069	0.986±0.050
6548.05	[NII]	-13.344±0.716	2.010±0.392	-13.296±0.014	1.674±0.050
6562.85	Hα	-12.765±0.443	2.226±0.330	-11.934±0.002	2.959±0.045
6583.45	[NII]	-13.351±0.011	2.449±0.181	-12.828±0.012	2.166±0.059
6678.15	HeI	-14.504±0.191	1.413±0.400	-13.853±0.022	1.585±0.206
7065.71	HeI	-	-	-13.723±0.038	1.767±0.109
7135.80	[ArIII]	-14.161±0.072	1.699±0.354	-	-

Table 6 M 1-5 fluxes and equivalent widths.

Wavelength Å	Ion	This Work		W05	
		log [Flux] (ergs cm ⁻² s ⁻¹)	log [EW] (Å)	log [Flux] (ergs cm ⁻² s ⁻¹)	log [EW] (Å)
4101.74	Hδ	-14.201±0.378	1.399±0.817	-	-
4340.47	Hγ	-14.199±0.000	2.263±0.079	-	-
4685.71	HeII	-13.681±0.004	2.332±0.207	-	-
4861.20	Hβ	-13.559±0.004	2.496±0.035	-	-
4958.52	[OIII]	-13.413±0.002	2.499±0.001	-	-
5007.57	[OIII]	-12.901±0.001	3.081±0.072	-	-
5269.20	[KVI]	-14.328±0.009	1.639±0.057	-	-
5754.59	[NII]	-14.555±0.035	1.385±0.122	-13.355±0.098	1.228±0.102
5875.97	HeI	-13.960±0.008	1.937±0.064	-12.551±0.007	2.029±0.062
6300.30	[OI]	-14.795±0.148	1.128±0.332	-13.273±0.032	1.265±0.038
6312.10	[SIII]	-	-	-13.685±0.034	0.819±0.048
6548.05	[NII]	-15.115±0.080	0.939±0.118	-12.086±0.002	1.793±0.076
6562.85	Hα	-12.703±0.013	3.018±0.063	-11.082±0.002	2.817±0.029
6583.45	[NII]	-13.216±0.018	2.510±0.026	-11.595±0.001	2.498±0.063
6678.15	HeI	-14.519±0.080	1.273±0.054	-12.940±0.001	1.572±0.032
6716.47	[SII]	-	-	-13.497±0.005	1.008±0.026
6730.85	[SII]	-14.730±0.028	1.22±0.058	-13.157±0.001	1.332±0.016
7065.71	HeI	-14.147±0.004	1.710±0.031	-12.513±0.002	1.942±0.031
7135.80	[ArIII]	-13.785±0.607	2.115±0.584	-12.530±0.010	1.919±0.045

Table 7 NGC6833 fluxes and equivalent widths.

Wavelength Å	Ion	This Work		W05	
		log [Flux] (ergs cm ⁻² s ⁻¹)	log [EW] (Å)	log [Flux] (ergs cm ⁻² s ⁻¹)	log [EW] (Å)
3697.15	H17	-	-	-13.829±0.241	0.000±0.109
3705.00	HeI	-	-	-13.288±0.081	0.423±0.037
3712.75	HeII	-	-	-13.346±0.149	0.401±0.043
3726.19	[OII]	-	-	-12.259±0.066	1.358±0.012
3734.37	H13	-	-	-12.977±0.116	0.562±0.024
3750.15	H12	-	-	-12.920±0.023	0.959±0.004
3770.63	H11	-	-	-12.812±0.024	1.066±0.005
3797.90	H10	-	-	-12.689±0.055	1.184±0.003
3819.70	HeI*	-	-	-13.305±0.146	0.573±0.076
3835.38	H9	-	-	-12.540±0.030	1.334±0.006
3868.71	[NeIII]	-	-	-11.439±0.020	2.394±0.033
3889.05	H8	-12.771±0.004	2.219±0.043	-12.142±0.019	1.692±0.024
3967.41	[NeIII]	-13.889±0.096	1.049±0.159	-11.761±0.001	2.136±0.005
4026.10	HeI*	-12.793±0.011	2.123±0.104	-13.025±0.013	0.905±0.014
4068.91	CIII	-	-	-13.442±0.128	0.481±0.117
4101.74	Hβ	-	-	-11.954±0.006	1.988±0.001
4340.47	Hγ	-12.947±0.004	1.788±0.020	-11.673±0.037	2.269±0.026
4363.21	[OIII]	-14.164±0.110	0.567±0.127	-12.247±0.040	1.715±0.056
4387.93	HeI	-	-	-13.601±0.042	0.378±0.006
4471.68	HeI	-	-	-12.613±0.039	1.369±0.030
4685.71	HeII	-13.699±0.070	1.018±0.107	-	-
4713.38	HeI*	-13.727±0.070	0.975±0.107	-13.244±0.009	0.821±0.012
4724.30	[NeIV]	-13.884±0.144	0.828±0.188	-	-
4740.18	[ArIV]	-	-	-13.447±0.034	0.590±0.039
4861.20	Hβ	-11.838±0.002	2.827±0.079	-11.315±0.012	2.733±0.033
4921.93	HeI	-13.587±0.095	1.057±0.155	-13.246±0.034	0.785±0.050
4958.52	[OIII]	-11.410±0.001	3.171±0.077	-10.886±0.007	3.003±0.023
5007.57	[OIII]	-11.075±0.000	3.397±0.074	-10.401±0.001	3.439±0.074
5191.80	[ArIII]	-	-	-14.275±0.177	-0.150±0.186
5269.20	[KVI]	-13.314±0.024	1.219±0.036	-	-
5537.89	[CIII]	-	-	-13.935±0.082	0.243±0.098
5754.59	[NII]	-13.314±0.024	1.219±0.036	-13.049±0.047	1.121±0.017
5875.97	HeI	-12.423±0.001	2.129±0.011	-12.038±0.002	2.112±0.011
6300.30	[OI]	-13.187±0.023	1.524±0.079	-12.841±0.268	1.342±0.272
6312.10	[SIII]	-13.671±0.037	1.113±0.068	-	-
6363.77	[OI]	-13.622±0.044	1.122±0.051	-13.245±0.006	0.966±0.080
6548.05	[NII]	-12.723±0.030	1.870±0.010	-12.262±0.007	1.247±0.038
6562.85	Hα	-11.371±0.001	3.320±0.144	-10.752±0.001	2.838±0.051
6583.45	[NII]	-12.239±0.001	2.367±0.013	-11.865±0.003	1.867±0.021
6678.15	HeI	-13.048±0.002	1.661±0.010	-12.620±0.007	1.598±0.028

Table 8 IC5117 fluxes and equivalent widths.

Wavelength Å	Ion	This Work		W05	
		log [Flux] (ergs cm ⁻² s ⁻¹)	log [EW] (Å)	log [Flux] (ergs cm ⁻² s ⁻¹)	log [EW] (Å)
3705.00	HeI	-	-	-13.661±0.155	0.810±0.211
3712.75	HeII	-	-	-13.656±0.032	0.806±0.122
3726.19	[OII]	-	-	-12.337±0.004	1.768±0.023
3734.37	H13	-	-	-13.340±0.088	0.493±0.261
3750.15	H12	-	-	-13.254±0.021	1.217±0.179
3770.63	H11	-	-	-13.156±0.053	1.502±0.051
3797.90	H10	-	-	-13.014±0.005	1.651±0.175
3819.70	HeI*	-	-	-13.700±0.001	0.846±0.019
3835.38	H9	-	-	-12.836±0.015	1.767±0.016
3868.71	[NeIII]	-	-	-11.503±0.002	2.871±0.071
3889.05	H8	-	-	-12.482±0.013	1.955±0.098
3967.41	[NeIII]	-	-	-11.844±0.003	2.781±0.100
4068.91	CIII	-	-	-12.991±0.002	1.382±0.063
4101.74	Hδ	-12.943±0.214	2.696±0.214	-12.179±0.012	2.387±0.134
4340.47	Hγ	-12.537±0.388	2.845±0.388	-11.876±0.003	2.581±0.112
4363.21	[OIII]	-12.832±0.328	2.752±0.328	-12.191±0.010	2.262±0.077
4471.68	HeI	-13.365±0.265	2.288±0.265	-12.798±0.001	1.783±0.024
4634.14	NIII	-13.542±0.624	1.209±0.624	-13.576±0.036	0.695±0.333
4640.64	NIII	-	-	-13.215±0.013	0.947±0.291
4685.71	HeII	-12.888±0.464	2.473±0.464	-12.359±0.001	2.106±0.075
4713.38	HeI*	-13.555±0.549	1.765±0.549	-13.036±0.003	1.419±0.082
4724.30	[NeIV]	-	-	-14.154±0.057	0.270±0.163
4740.18	[ArIV]	-13.175±0.206	2.047±0.206	-12.661±0.001	1.813±0.029
4861.20	Hβ	-11.873±0.212	3.331±0.212	-11.380±0.020	3.032±0.006
4921.93	HeI	-13.644±0.448	1.442±0.448	-13.180±0.050	1.019±0.063
4958.52	[OIII]	-11.093±0.187	3.687±0.187	-10.629±0.023	3.270±0.124
5007.57	[OIII]	-10.646±0.294	3.560±0.294	-10.131±0.017	3.743±0.026
5191.80	[ArIII]	-	-	-14.152±0.159	0.151±0.004
5197.90	[NI]	-	-	-13.852±0.019	0.488±0.116
5411.52	HeII	-13.519±0.094	1.361±0.094	-13.276±0.042	1.107±0.019
5517.72	[CIII]	-	-	-14.084±0.025	0.209±0.072
5537.89	[CIII]	-13.635±0.005	1.138±0.005	-13.544±0.005	0.801±0.007
5754.59	[NII]	-12.931±0.048	1.798±0.048	-12.653±0.006	1.650±0.005
5875.97	HeI	-	-	-11.909±0.024	2.325±0.109
6300.30	[OI]	-12.638±0.056	2.155±0.056	-12.177±0.026	1.881±0.050
6312.10	[SIII]	-13.010±0.057	1.868±0.057	-12.606±0.039	1.437±0.011
6363.77	[OI]	-13.073±0.153	1.756±0.153	-12.656±0.024	1.453±0.038
6548.05	[NII]	-12.245±0.119	2.398±0.119	-11.733±0.032	1.612±0.116
6562.85	Hα	-11.024±0.162	3.588±0.162	-10.524±0.002	2.887±0.223
6583.45	[NII]	-11.781±0.117	2.797±0.117	-11.272±0.008	2.312±0.184

PASA (2018)

doi:10.1017/pas.2018.x

Table 9 Hu 1-1 fluxes and equivalent widths.

Wavelength Å	Ion	log [Flux] (ergs cm ⁻² s ⁻¹)	log [EW] (Å)
3726.19	[OII]	-11.424±0.002	2.967±0.018
3797.90	H10	-13.353±0.011	1.217±0.006
3835.38	H9	-13.065±0.006	1.519±0.005
3868.71	[NeIII]	-11.768±0.005	2.776±0.094
3889.05	H8	-12.524±0.023	2.160±0.142
3967.41	[NeIII]	-12.108±0.011	2.727±0.239
4026.10	HeI*	-13.547±0.057	1.258±0.007
4068.91	CIII	-12.929±0.020	1.848±0.064
4101.74	Hδ	-12.416±0.008	2.352±0.065
4340.47	Hγ	-12.163±0.012	2.607±0.168
4363.21	[OIII]	-12.743±0.044	2.027±0.200
4471.68	HeI	-13.010±0.084	1.676±0.213
4640.64	NIII	-13.518±0.080	1.187±0.058
4685.71	HeII	-12.498±0.035	2.677±0.695
4713.38	HeI*	-13.574±0.064	2.469±0.048
4861.20	Hβ	-11.793±0.001	2.953±0.035
4921.93	HeI	-13.408±0.040	1.334±0.068
4959.52	[OIII]	-11.179±0.002	3.500±0.186
5007.57	[OIII]	-10.734±0.001	3.811±0.158
5197.90	[NI]	-13.375±0.159	1.479±0.181
5411.52	HeII	-13.449±0.074	1.337±0.099
5537.89	[CIII]	-13.109±0.063	1.910±0.286
5875.97	HeI	-12.539±0.005	2.346±0.046
6300.30	[OI]	-12.378±0.008	2.540±0.014
6363.77	[OI]	-12.856±0.008	2.101±0.039
6562.85	Hα	-10.912±0.001	1.583±0.002
6678.15	HeI	-13.126±0.019	1.763±0.061
6730.85	[SII]	-11.911±0.002	2.972±0.050
7065.71	HeI	-13.104±0.011	1.826±0.038
7135.80	[ArIII]	-12.384±0.003	2.550±0.037

Table 10 M 1-4 fluxes and equivalent widths.

Wavelength Å	Ion	log [Flux] (ergs cm ⁻² s ⁻¹)	log [EW] (Å)
4861.20	H β	-12.610 \pm 0.087	1.350 \pm 0.183
4959.52	[OIII]	-11.942 \pm 0.021	1.930 \pm 0.104
5007.57	[OIII]	-11.462 \pm 0.007	2.456 \pm 0.108
5875.97	HeI	-12.845 \pm 0.003	1.883 \pm 0.013
6300.30	[OI]	-14.304 \pm 0.056	0.469 \pm 0.085
6312.10	[SIII]	-13.670 \pm 0.011	0.469 \pm 0.085
6562.85	H α	-11.443 \pm 0.001	3.130 \pm 0.056
6583.45	[NII]	-12.854 \pm 0.022	1.729 \pm 0.071
6678.15	HeI	-13.292 \pm 0.048	1.233 \pm 0.086
6716.47	[SII]	-13.878 \pm 0.015	0.665 \pm 0.003
6730.85	[SII]	-13.810 \pm 0.304	0.714 \pm 0.378
7065.71	HeI	-12.973 \pm 0.054	1.519 \pm 0.134
7135.80	[ArIII]	-12.820 \pm 0.020	1.670 \pm 0.063

Table 11 K 3-70 fluxes and equivalent widths.

Wavelength Å	Ion	log [Flux] (ergs cm ⁻² s ⁻¹)	log [EW] (Å)
4959.52	[OIII]	-13.546 \pm 0.005	2.871 \pm 0.239
5007.57	[OIII]	-13.045 \pm 0.001	3.276 \pm 0.164
5754.59	[NII]	-14.256 \pm 0.042	2.030 \pm 0.309
5875.97	HeI	-14.360 \pm 0.009	2.125 \pm 0.147
6300.30	[OI]	-14.815 \pm 0.087	1.648 \pm 0.135
6312.10	[SIII]	-14.994 \pm 0.094	1.958 \pm 0.653
6548.05	[NII]	-13.204 \pm 0.001	3.465 \pm 0.080
6562.85	H α	-13.130 \pm 0.004	3.046 \pm 0.289
6583.45	[NII]	-12.720 \pm 0.002	3.306 \pm 0.245
6678.15	HeI	-14.903 \pm 0.053	1.932 \pm 0.486
6716.47	[SII]	-14.440 \pm 0.051	1.858 \pm 0.258
6730.85	[SII]	-14.293 \pm 0.005	2.160 \pm 0.077
7065.71	HeI	-14.555 \pm 0.045	2.090 \pm 0.341
7135.80	[ArIII]	-14.139 \pm 0.006	2.515 \pm 0.204

Table 12 M 1-17 fluxes and equivalent widths.

Wavelength Å	Ion	log [Flux] (ergs cm ⁻² s ⁻¹)	log [EW] (Å)
4861.20	Hβ	-12.734±0.004	3.201±0.391
4959.52	[OIII]	-12.014±0.001	3.751±0.415
5007.57	[OIII]	-11.511±0.000	4.007±0.211
5197.90	[NI]	-14.116±0.098	1.748±0.371
5754.59	[NII]	-13.645±0.116	2.026±0.662
5875.97	HeI	-13.218±0.013	2.294±0.174
6300.30	[OI]	-13.177±0.005	2.361±0.027
6312.10	[SIII]	-13.948±0.057	1.609±0.244
6363.77	[OI]	-13.601±0.001	1.940±0.001
6548.05	[NII]	-12.529±0.000	2.919±0.002
6562.85	Hα	-11.948±0.000	3.462±0.001
6583.45	[NII]	-12.101±0.004	3.361±0.236
6678.15	HeI	-13.813±0.009	1.835±0.460
6716.47	[SII]	-13.363±0.004	2.248±0.076
6730.85	[SII]	-13.144±0.001	2.486±0.044
7065.71	HeI	-13.558±0.011	1.909±0.092
7135.80	[ArIII]	-12.968±0.000	2.516±0.002

Table 13 SaSt 2-3 fluxes and equivalent widths.

Wavelength Å	Ion	log [Flux] (ergs cm ⁻² s ⁻¹)	log [EW] (Å)
4068.91	CIII	-13.812±0.027	0.701±0.035
4713.38	HeI*	-14.145±0.018	0.191±0.022
4861.20	Hβ	-12.694±0.001	1.599±0.002
5007.57	[OIII]	-14.115±0.002	0.166±0.002
5754.59	[NII]	-14.241±0.047	0.007±0.001
6300.30	[OI]	-13.715±0.007	0.748±0.015
6548.05	[NII]	-12.942±0.002	1.615±0.009
6562.85	Hα	-12.114±0.000	2.534±0.003
6583.45	[NII]	-12.553±0.001	2.093±0.007
6716.47	[SII]	-13.900±0.008	0.684±0.012
6730.85	[SII]	-13.723±0.007	0.863±0.008
7135.80	[ArIII]	-14.719±0.007	0.783±0.016

Table 14 H 4-1 fluxes and equivalent widths.

Wavelength Å	Ion	log [Flux] (ergs cm ⁻² s ⁻¹)	log [EW] (Å)
3712.75	HeII	-12.403±0.004	2.687±0.093
3734.37	H13	-14.359±0.052	0.837±0.053
3750.15	H12	-14.125±0.067	1.170±0.158
3770.63	H11	-13.918±0.004	1.439±0.007
3819.70	HeI*	-13.731±0.016	1.652±0.049
3835.38	H9	-13.823±0.008	1.545±0.020
3868.71	[NeIII]	-13.226±0.000	2.132±0.003
4068.91	CIII	-13.181±0.010	2.329±0.122
4340.47	H γ	-12.954±0.003	2.537±0.060
4363.21	[OIII]	-13.698±0.025	1.774±0.109
4387.93	HeI	-14.709±0.074	0.809±0.093
4471.68	HeI	-13.887±0.042	1.583±0.127
4685.71	HeII	-13.567±0.011	2.079±0.091
4861.20	H β	-12.570±0.000	3.252±0.014
4921.93	HeI	-14.177±0.006	1.549±0.014
4959.52	[OIII]	-12.247±0.000	3.332±0.014
5007.57	[OIII]	-11.773±0.000	3.746±0.099
5197.90	[NI]	-14.359±0.052	1.272±0.022
5411.52	HeII	-14.525±0.067	1.049±0.017
5754.59	[NII]	-14.249±0.005	1.532±0.004
6300.30	[OI]	-14.290±0.065	1.308±0.041
6363.77	[OI]	-13.950±0.044	1.753±0.169
6548.05	[NII]	-13.018±0.153	2.026±0.937
6562.85	H α	-12.060±0.017	3.013±0.858
6583.45	[NII]	-12.452±0.010	2.921±0.439
6678.15	HeI	-13.875±0.038	1.946±0.226
6716.47	[SII]	-14.518±0.029	1.136±0.049
6730.85	[SII]	-14.534±0.049	1.119±0.099
7065.71	HeI	-13.820±0.011	1.869±0.064
7135.80	[ArIII]	-14.634±0.003	1.115±0.007

Table 15 DdDm 1 fluxes and equivalent widths.

Wavelength Å	Ion	log [Flux] (ergs cm ⁻² s ⁻¹)	log [EW] (Å)
5875.97	HeI	-14.549±0.151	2.163±0.247
6300.30	[OI]	-14.871±0.069	1.998±0.623
6312.10	[SIII]	-15.104±0.109	1.508±0.414
6548.05	[NII]	-13.346±0.002	3.233±0.303
6562.85	H α	-13.247±0.001	3.258±0.278
6583.45	[NII]	-12.847±0.000	3.668±0.229
6678.15	HeI	-15.090±0.027	1.697±0.192
6716.47	[SII]	-14.480±0.001	2.499±0.046
6730.85	[SII]	-14.331±0.006	2.458±0.265
7065.71	HeI	-14.736±0.017	2.693±0.841
7135.80	[ArIII]	-14.245±0.002	3.372±0.627

Table 16 Na 1 fluxes and equivalent widths.

Wavelength Å	Ion	log [Flux] (ergs cm ⁻² s ⁻¹)	log [EW] (Å)
3726.19	[OII]	-13.408±0.053	1.270±0.078
3868.71	[NeIII]	-12.329±0.004	2.348±0.038
3889.05	H8	-13.090±0.033	1.551±0.074
3967.41	[NeIII]	-12.681±0.011	2.081±0.066
4101.74	Hδ	-12.908±0.017	1.895±0.060
4340.47	Hγ	-12.660±0.001	2.135±0.002
4363.21	[OIII]	-13.133±0.019	1.667±0.056
4471.68	HeI	-13.481±0.168	1.396±0.286
4640.64	NIII	-13.409±0.004	1.526±0.000
4685.71	HeII	-12.997±0.019	1.849±0.072
4713.38	HeI*	-13.479±0.076	1.353±0.141
4740.18	[ArIV]	-13.602±0.112	1.242±0.180
4861.20	Hβ	-12.175±0.003	2.759±0.062
4959.52	[OIII]	-11.497±0.001	3.216±0.071
5007.57	[OIII]	-11.014±0.001	3.659±0.178
5197.90	[NI]	-14.205±0.520	0.708±0.585
5411.52	HeII	-13.913±0.005	0.920±0.006
5875.97	HeI	-12.692±0.001	2.113±0.006
6300.30	[OI]	-14.600±0.118	0.332±0.146
6312.10	[SIII]	-14.048±0.014	0.832±0.012
6562.85	Hα	-11.419±0.000	3.417±0.024
6583.45	[NII]	-13.347±0.045	1.477±0.079
6678.15	HeI	-13.235±0.020	1.626±0.056
6730.85	[SII]	-13.748±0.061	1.136±0.085
7065.71	HeI	-13.227±0.004	1.639±0.013
7135.80	[ArIII]	-13.013±0.003	1.858±0.011

Table 17 Vy 1-2 fluxes and equivalent widths.

Wavelength Å	Ion	log [Flux] (ergs cm ⁻² s ⁻¹)	log [EW] (Å)
3750.15	H12	-12.118±0.011	1.832±0.043
3797.90	H10	-12.631±0.001	1.567±0.048
3819.70	HeI*	-12.895±0.036	1.420±0.095
3868.71	[NeIII]	-12.795±0.010	1.417±0.029
3889.05	H8	-11.578±0.003	2.655±0.014
4026.10	HeI*	-13.224±0.010	1.198±0.018
4068.91	CIII	-13.000±0.020	1.396±0.034
4101.74	Hδ	-12.120±0.007	2.313±0.069
4340.47	Hγ	-11.928±0.002	2.496±0.025
4363.21	[OIII]	-12.638±0.007	1.766±0.013
4471.68	HeI	-12.938±0.060	1.551±0.162
4634.14	NIII	-12.767±0.069	1.721±0.171
4685.71	HeII	-12.101±0.008	2.341±0.107
4713.38	HeI*	-12.926±0.082	1.532±0.217
4740.18	[ArIV]	-12.992±0.061	1.497±0.163
4861.20	Hβ	-11.552±0.005	2.981±0.215
4921.93	HeI	-12.860±0.007	1.754±0.003
4959.52	[OIII]	-11.052±0.003	3.369±0.241
5007.57	[OIII]	-10.700±0.002	3.711±0.253
5411.52	HeII	-13.088±0.019	1.679±0.055
5875.97	HeI	-12.326±0.014	2.466±0.160
6300.30	[OI]	-13.238±0.057	1.547±0.082
6312.10	[SIII]	-13.242±0.028	1.641±0.191
6363.77	[OI]	-13.685±0.016	1.080±0.027
6548.05	[NII]	-12.576±0.045	2.071±0.008
6562.85	Hα	-11.201±0.000	3.496±0.121
6583.45	[NII]	-12.147±0.005	2.630±0.114
6678.15	HeI	-12.973±0.006	1.808±0.026
6716.47	[SII]	-13.163±0.023	1.634±0.066
6730.85	[SII]	-12.954±0.003	1.820±0.011
7065.71	HeI	-12.973±0.001	1.823±0.007
7135.80	[ArIII]	-12.394±0.002	2.384±0.021

Table 18 M 3-27 fluxes and equivalent widths.

Wavelength Å	Ion	log [Flux] (ergs cm ⁻² s ⁻¹)	log [EW] (Å)
3770.63	H11	-12.014±0.003	2.182±0.023
3797.90	H10	-12.964±0.038	1.222±0.066
3967.41	[NeIII]	-13.296±0.013	0.926±0.019
4026.10	HeI*	-13.161±0.055	1.090±0.076
4068.91	CIII	-12.760±0.014	1.479±0.033
4340.47	Hγ	-12.513±0.023	1.761±0.086
4363.21	[OIII]	-12.031±0.011	2.251±0.098
4471.68	HeI	-12.978±0.056	1.320±0.107
4713.38	HeI*	-13.521±0.138	0.753±0.168
4861.20	Hβ	-11.930±0.004	2.353±0.041
4921.93	HeI	-13.377±0.040	0.946±0.054
5875.97	HeI	-12.186±0.014	2.164±0.146
6300.30	[OI]	-12.471±0.001	1.845±0.031
6312.10	[SIII]	-12.841±0.013	1.634±0.001
6363.77	[OI]	-12.710±0.035	1.685±0.117
6548.05	[NII]	-10.958±0.002	2.395±0.015
6562.85	Hα	-10.607±0.001	3.417±0.160
6678.15	HeI	-12.887±0.049	1.328±0.121
6730.85	[SII]	-12.671±0.097	0.729±0.111
7065.71	HeI	-12.195±0.003	2.083±0.024
7135.80	[ArIII]	-12.997±0.047	1.339±0.117

Table 19 IC 4997 fluxes and equivalent widths.

Wavelength Å	Ion	log [Flux] (ergs cm ⁻² s ⁻¹)	log [EW] (Å)
3734.37	H13	-11.186±0.057	2.102±0.307
3770.63	H11	-12.230±0.080	1.051±0.161
3797.90	H10	-11.917±0.053	1.364±0.137
3819.70	HeI*	-11.788±0.026	1.508±0.085
3835.38	H9	-12.395±0.120	0.882±0.188
3868.71	[NeIII]	-10.466±0.002	2.813±0.079
3889.05	H8	-11.290±0.013	1.968±0.101
3967.41	[NeIII]	-10.790±0.002	2.450±0.039
4026.10	HeI*	-12.143±0.039	1.109±0.080
4068.91	CIII	-11.959±0.064	1.338±0.124
4101.74	Hδ	-11.105±0.007	2.182±0.080
4340.47	Hγ	-10.878±0.001	2.419±0.028
4363.21	[OIII]	-10.822±0.004	2.468±0.095
4387.93	HeI	-12.580±0.010	0.872±0.001
4471.68	HeI	-11.770±0.015	1.603±0.060
4640.64	NIII	-12.296±0.071	1.120±0.003
4713.38	HeI*	-12.384±0.016	0.999±0.030
4740.18	[ArIV]	-12.571±0.274	0.883±0.366
4861.20	Hβ	-10.587±0.002	2.742±0.066
4921.93	HeI	-12.309±0.057	1.049±0.100
4959.52	[OIII]	-10.342±0.002	2.959±0.090
5007.57	[OIII]	-9.947±0.002	3.306±0.190
5754.59	[NII]	-12.380±0.008	1.156±0.017
5875.97	HeI	-11.122±0.004	2.393±0.051
6300.30	[OI]	-11.638±0.011	1.874±0.067
6312.10	[SIII]	-11.937±0.010	1.561±0.063
6363.77	[OI]	-12.103±0.004	1.348±0.010
6548.05	[NII]	-11.451±0.010	1.912±0.069
6562.85	Hα	-10.038±0.000	3.315±0.064
6583.45	[NII]	-11.050±0.006	2.294±0.087
6678.15	HeI	-11.714±0.008	1.749±0.049
6716.47	[SII]	-12.464±0.059	1.002±0.103
6730.85	[SII]	-12.176±0.007	1.273±0.017
7065.71	HeI	-11.229±0.002	2.239±0.037
7135.80	[ArIII]	-11.343±0.001	2.123±0.019

Table 20 Me 2-2 fluxes and equivalent widths.

Wavelength Å	Ion	log [Flux] (ergs cm ⁻² s ⁻¹)	log [EW] (Å)
3734.37	H13	-11.865±0.002	1.839±0.007
3770.63	H11	-12.898±0.033	0.881±0.060
3819.70	HeI*	-12.579±0.031	1.280±0.071
3835.38	H9	-12.990±0.104	0.887±0.159
3868.71	[NeIII]	-11.402±0.002	2.492±0.033
3889.05	H8	-11.958±0.002	1.946±0.036
3967.41	[NeIII]	-11.688±0.003	2.259±0.037
4026.10	HeI*	-12.668±0.013	1.289±0.032
4101.74	Hδ	-11.796±0.003	2.145±0.034
4340.47	Hγ	-11.555±0.003	2.432±0.056
4363.21	[OIII]	-12.438±0.023	1.547±0.079
4387.93	HeI	-13.299±0.150	0.730±0.185
4471.68	HeI	-12.308±0.031	1.804±0.165
4713.38	HeI*	-12.974±0.034	1.089±0.060
4740.18	[ArIV]	-13.405±0.015	0.686±0.015
4861.20	Hβ	-11.163±0.002	2.885±0.093
4921.93	HeI	-12.845±0.020	1.201±0.039
4959.52	[OIII]	-10.778±0.007	3.196±0.040
5007.57	[OIII]	-10.323±0.001	3.600±0.043
5191.80	[ArIII]	-13.212±0.100	0.948±0.152
5537.89	[CIII]	-13.483±0.007	0.725±0.003
5754.59	[NII]	-13.811±0.014	0.368±0.003
5875.97	HeI	-11.650±0.004	2.472±0.091
6300.30	[OI]	-12.688±0.021	1.511±0.071
6312.10	[SIII]	-13.190±0.117	0.977±0.208
6363.77	[OI]	-13.103±0.051	1.119±0.102
6548.05	[NII]	-11.350±0.004	2.719±0.160
6562.85	Hα	-10.590±0.001	3.489±0.182
6583.45	[NII]	-10.860±0.002	3.296±0.082
6678.15	HeI	-12.280±0.005	1.896±0.057
6716.47	[SII]	-13.236±0.001	1.024±0.002
6730.85	[SII]	-13.116±0.031	1.094±0.051
7065.71	HeI	-11.831±0.003	2.354±0.057
7135.80	[ArIII]	-12.056±0.006	2.128±0.076

Table 21 Vy 2-3 fluxes and equivalent widths.

Wavelength Å	Ion	log [Flux] (ergs cm ⁻² s ⁻¹)	log [EW] (Å)
3750.15	H12	-12.104±0.010	1.733±0.025
3889.05	H8	-12.559±0.013	1.317±0.025
4068.91	CIII	-12.630±0.012	1.270±0.020
4340.47	H γ	-12.393±0.003	1.576±0.006
4363.21	[OIII]	-13.169±0.020	0.803±0.025
4471.68	HeI	-13.326±0.080	0.659±0.094
4685.71	HeII	-13.776±0.073	0.222±0.079
4713.38	HeI*	-13.707±0.034	0.300±0.037
4861.20	H β	-11.997±0.002	2.047±0.012
4959.52	[OIII]	-11.486±0.001	2.562±0.016
5007.57	[OIII]	-11.053±0.000	2.993±0.010
5875.97	HeI	-12.686±0.016	1.568±0.043
6562.85	H α	-11.436±0.001	2.938±0.027
6583.45	[NII]	-13.527±0.009	0.865±0.017
6678.15	HeI	-13.252±0.011	1.179±0.019
7065.71	HeI	-13.328±0.015	1.168±0.025
7135.80	[ArIII]	-12.980±0.003	1.520±0.008